On-Site Rapid Detection of Ethidium Bromide Using Ultramicroelectrode Sensors

[1]Marcello Valente., [1]Ian Seymour, [1]Md Ridwan Adib, [1]Tarun Narayan, [2]Valentina Alessandria, [2]Luca Cocolin , [3]Kieran G Meade , [1]Alan O'Riordan

[Chemosensors] (IF: 4.2) Special Issue "Rapid Point-of-Care Testing Technology and Application"

1 Tyndall National institute, UCC, Cork, Ireland

2 DISAFA., University of Turin, Grugliasco, Italy

3 UCD School of Agriculture and Food Science, University College Dublin, Belfield, D04 V1W8, Dublin, Ireland.
UCD Conway Institute of Biomolecular and Biomedical Research, University College Dublin, Belfield, D04 V1W8, Dublin, Ireland.

Abstract

Ethidium bromide (EtBr) is one of the most used non-protein molecules in molecular biology, specifically for fluorescence-based detection of nucleic acids during gel electrophoresis. ETBr2 fluoresces when exposed to ultraviolet light, intensifying after binding to DNA. Although non-radioactive, the ability of EtBr to bind preferentially to the double strand structure and to enter the nucleus membrane of cells makes it a toxic substance, which can cause tumorigenesis due to the genetic damage induced by its interaction. Its reputation as a potential mutagen has created a need to minimize its use and eliminate the risks associated with exposure, as well as the potential environmental hazards associated with disposal. In the last 10 years, EtBr has also been shown to be electrochemically active. In this work, we show the modification of an ultra-micro electrode sensor and subsequent detection of EtBr from Phosphate buffer on a nanomolar level (LoD of 12 nM). The sensor can detect concentrations with a higher sensitivity and reliability than the classic UV lamp in a practical manner. This novel sensor may offer a potential solution to test for and reduce potentials risks associated with both job related risk and unwanted environmental release of EtBr.

Introduction

Many molecules of the phenanthridine group are used as fluorescence tags in gel electrophoresis due to their high quantum efficiencies and stability [1], [2], [3]. Ethidium bromide (EtBr) is one of the most used phenanthridine compounds, due to its ability to bind nucleic acids, and has been documented in

the literature since 1964 [4]. It is typically seen as the gold standard of the florescence tags [5] used for gel electrophoresis [6], [7], [8]. More recently it is being used to assess anti-toxicity studies in bacteria [9]. The ability of EtBr to bind to DNA comes with caution since it has also been shown to stop the nucleic acids synthesis in *Strigomonas oncopelti* [10], damage the mitochondrial circular DNA [11], [12], [13]and cause mutations in DNA [14]. Despite these negatives, ethidium bromide is still a well-used dye [15] with it ability to bind to different sites on the dsDNA, for which it has a preference, and also to ssDNA structures [16], [17]. Recently, EtBr is also used as an electrochemical probe molecule [18]. The oxidation of EtBr has been studied using cyclic voltammetry on these, on a variety of working electrode materials such as boron-doped diamond [19] mercury drop systems [20] and large gold electrodes [21] and has been used to electrochemically detect EtBr that is bound to DNA complementing fluorescence approaches[22].

EtBr has also been used as a pest control with the toxicity of molecule gaining awareness in 1970s. EtBr was shown to cause consistent damage to mitochondrial [23], [24], [25], [26] ribosomal DNA [27] and non-nuclear DNA in different models leading to neurodegenerative disorders and higher risk of tumorigenesis [28], [29] [30]. Long term effects of EtBr induced mitochondrial DNA damage leading to rapid cellular ageing [31] for the single individual and call also lead to infertility or other reproductive problems in animal models specifically infertility or early menopause [32], [33] or spontaneous abortion [34] while damage to Male sperm's mitochondria is also possible [35]. To this end, the risk for mitochondrial has resulted in stringent Health & Safety procedures regarding EtBr use and, more specifically, concerning its disposal and detection [36]. Concerning electrochemical detection of EtBr, reports in the literature exhibit limits of detection typically in the micro molar concentrations of range. This limitation of detection may not be fit-for-purpose for on-site detection as smaller concentrations of this substance may cause damage over time; thereby highlighting the need for a more sensitive detection method [37], [38]. To date, electrochemical methods have been more successfully applied to remediation of the molecule [39], [40], [41] rather than detection.

In this work, we develop a sensitive electrochemical based sensor, incorporating solid-state ultramicroelectrode sensors, that allows detection of EtBr contamination (nanomolar) in real time and apply this to the detection of EtBr of swab samples from a microbiology laboratory. Our approach is shown schematically in Figure 1. First a cotton swab is wiped across to the area under test and then immersed in 0.5 mL of phosphate buffer and let stand for 5 minutes. The buffer is then agitated to ensure a homogeneous mixture and the placed into the sample well of a chip holder. Electrochemical analysis is then undertaken, and an EtBr concentration (time to result) obtained after 12 seconds. The approach is rapid and yields quantitative results unlike current approaches using dyes or a UV lamp [42].

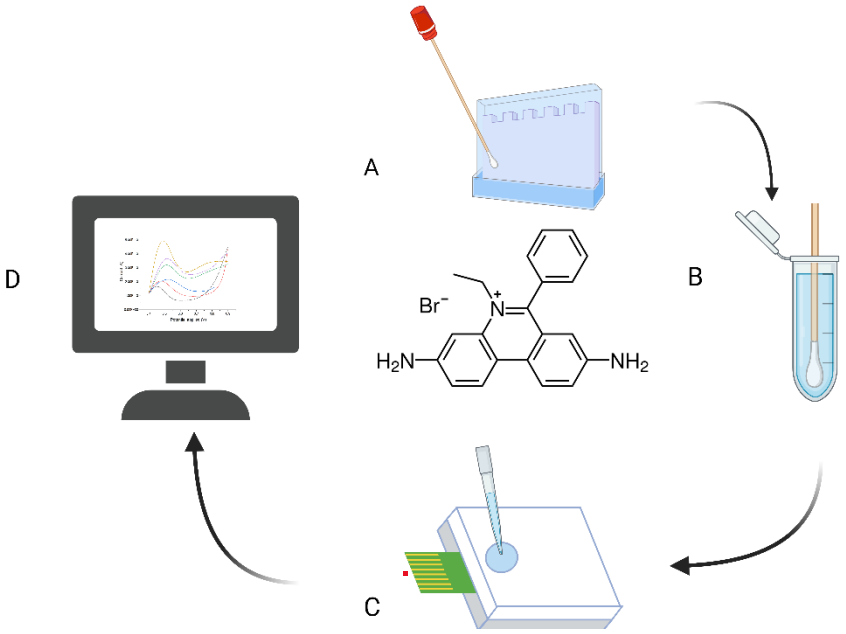

Fig. 1 schematic showing EtBr detection approach. (A) swabbing and sampling of surfaces with different potential levels of contamination risk e.g., the sample is taken from the surface where a spill or a surface where contamination is present, (B) the head of a swab is then immerse in 500 µL of phosphate buffer pH 7, (C) the liquid is transferred to the sample well of a sensor chip holder (D) analysis is undertaken and displayed visually in twelve seconds.

Material and methods

Chemicals

EtBr 1% solutions, sodium phosphate dibasic heptahydrate, sodium phosphate monobasic monohydrate, ferrocene carboxylic acid?, PBS tablets, AuCl trihydrate, sodium acetate and acetic acid (Sigma-Aldrich) were used for XXX. 10 mM phosphate buffer (PB) was prepared by dissolving 1 tablet in 250 mL with deionized water (Elgapure, 10^{18} Ω). EtBr 1% solutions were then diluted with PB to prepare a stock solution of 512 nM which was then further diluted to prepare standard solutions of 256 nM, 128 nM, 64 nM, 32 nM, 16 nM and 8 nM.

Electrochemical deposition and analysis

Chronoamperometry was employed to deposit nanogold on the electrode surfaces using an optimized voltage for a set time (see results section) . Cyclic Voltammetry (CV) and electrochemical impedance spectroscopy (EIS) was employed for electrode characterization, while square wave voltammetry was used for EtBr detection. All electrochemical analysis was undertaken using a multi-autolab M101 operating under Nova 1.0.4 software control (Netherlands). Electrochemical deposition employed an off-chip Ag/AgCl reference electrode and on-chip counter electrode, while the EtBr detection was undertaken using the on-chip Pt pseudo-reference and on-chip gold counter electrodes.

Atomic force microscopy

Sensor Fabrication

Silicon Chip fabrication was undertaken as described in previous publications[43], [44], [45], [46], [47], [48], [49]. In brief, four-inch silicon wafer substrates bearing a 300 nm thermally grown silicon dioxide layer were used. Working electrodes were first fabricated using optical lithography, metal evaporation (Ti 10 nm /Au 50 nm Temescal FC-2000 beam evaporator) and lift-off techniques to yield well-defined, stacked metallic (Ti/Au) microband (1 µm width, 50 nm height, 45 µm length) structures. Optical lithography and metal deposition (Ti 10 nm/Ni 70 nm/Au 200 nm) process was again undertaken to define a MicroSD pin-out, on-chip metal interconnection tracks, as well as counter and reference electrodes. Finally, a passivation Si_3N_4 layer was deposited on the chip by PECVD, with windows opened in this layer directly above the working, reference and counter electrodes and SD pinouts. The windows defined the length of the working electrode to be 45 µm. A PCB bearing a mounted microSD port connector structure was designed and fabricated to allow facile connection between the microSD primary contact pads with the potentiostat. In this manner, the microSD electrical pin-out enabled rapid and easy electrical connection to external electronics, enabling sensors to be used as a portable field sensor. Each silicon chip comprised six independent sensors containing two interdigitated electrode (IDE) structures, a platinum counter electrode, and a platinum pseudo-reference electrode. Gold contact pads and interconnection metallisation on two sides of the chip allowed electrical connection to both interdigitated structures. Figure 2 shows an optical micrography of a fully fabricated chip (based on previous designs) the SEM image shows a high-resolution image of a typical sensor device [29] [30]. IDEs were selected due to possibility of using localized pH control of the solutions for the ethidium bromide should this be required [43]. Finally. a custom-made holder cell constructed from an aluminium base and a Teflon™ lid was fabricated to allow measurement in small electrolyte volumes (≈500 µL). The cell was included a Viton O-ring, chosen for their chemical resistance, embedded in the lid which formed a seal around the on-chip electrodes. The inner diameter of the O-ring was 7 mm with a cross section of 1.6 mm which was of sufficient size to expose all six sensors, counter, and reference electrodes on the device to the electrolyte [43], [44].

Electrochemical characterization

Cyclic voltammetry (CV) was performed in 10 mM ferrocenecarboxylic acid (FCA) in 10 mM phosphate buffered saline (PBS) in the voltage range 0 -0 .6 V @ 100 mV s^{-1} using a commercial Ag/AgCl (Alvateck)

external reference electrode. CVs were also undertaken in Ethidium bromide solutions in the voltage range 0 to -0 .6 V @ 100 mV s^{-1} using the on-chip platinum pseudo-reference electrode. A Square wave voltammetry protocol for detection of Ethidium bromide was developed with the conditions 22 mV/s and 10 mV amplitude versus the platinum on-chip reference electrode.

.

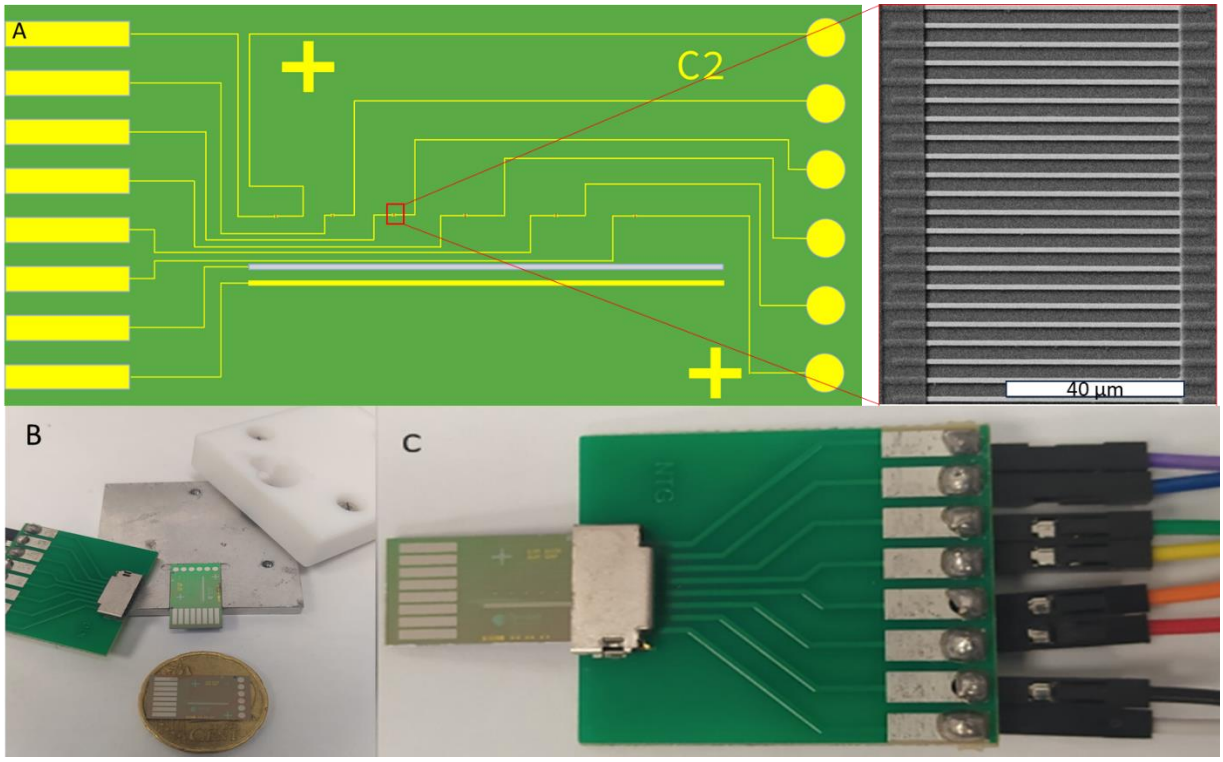

Fig. 2 (a) Structure of the sensor chip with a SEM zoom on the structure of the Working Electrode (b) Chip dimension comparison and relative holder and connector (c) Zoom on the SD chip connector.

Swabbing of contaminated surfaces

Surfaces were swabbed using a dry cotton swab over a ~20 x 20 cm area (400 cm^2) for ~1 min (to ensure full loading of the swab). The head of the swab was then immersed in 500 uL of 10 mM sodium phosphate solution at pH 7 in a Eppendorf tube, closed and sealed with parafilm and stored prior to measurement. To undertake analysis, the Eppendorf tube was placed on a shaker for few seconds, then an aliquot of 500 µL was removed and pipetted directly onto a chip mounted in the chip holder and analyzed by CV.

Results

Initial experiments for detection of ethidium bromide were undertaken using fabricated chips. However, due to the smoothness of the gold electrode it was not possible to achieve an electrochemical response despite previous reports in the literature [50]. Following a review, it was theorized that a roughened gold surface with sufficient nucleation points was required for ethidium bromide absorption thereby allowing electron transfer to occur. To this end, electrode modification was undertaken initially using amperometry (E= -0.3 V, 80 s) in a solution of 400 ppm gold chloride in sodium phosphate buffer at pH 3. Figure 3(a) shows a SEM image of a typical gold deposition, exhibiting sharp "nanospike" structures at the edges of the electrodes. While this approach did roughen the surface, the formation of these nanospikes was stochastic and formed gold overlaps between the interdigitated electrodes resulting in short circuits with a consequent reduction in the overall yield of devices. To address this, a chronopotentiometric method was developed and the optimized protocol of applying 24 nA for 200 s resulted in a stable 0.4 um nanogold deposition on the working electrodes. All six sensors on a chip were electroplated simultaneously by temporarily electrically shorting them together. Figure 3(b) shows a typical SEM image obtained using the chronopotentiometric method. It is evident from the image that the gold deposited uniformly across the electrodes and no bridging between electrodes was observed.

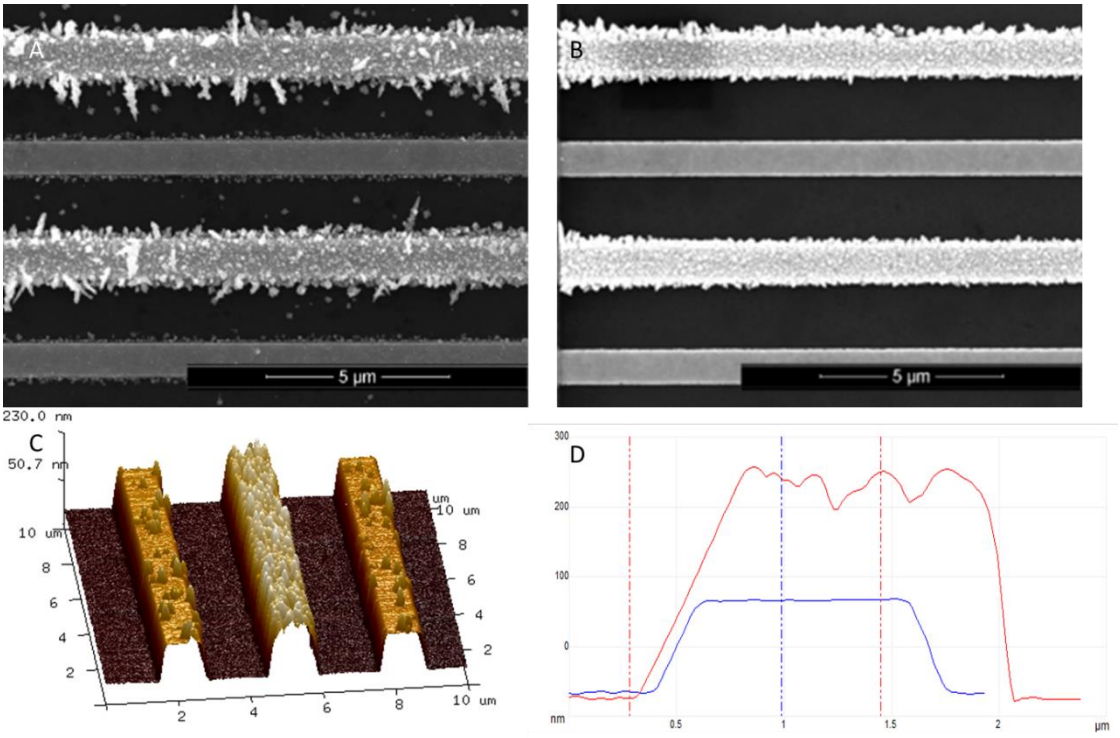

Fig. 3 SEM analysis of the working electrode interdigitated structure after the AuCl deposition. In (a) the amperometric over deposition on the interdigitated structure and the Imperfect depositions as the over deposition on the counterpart of the interdigitated working electrode. On the upper right the SEM of the deposition using chronopotentiometry in which the surface is deposited in a more coherent way and without the overdeposition in the other comb of interdigitated electrodes. In the lower images we can observe the AFM profiles of the rod deposited via chronopotentiometric protocol.

Electrochemical characterization was undertaken before and after electrode modification. Figure 4(a) shows typical CVs for both unmodified and modified electrodes. The bare gold electrodes exhibited quasi steady state behavior (black data) with a diffusion limited peak profile and increased hysteresis when compared to single microband electrodes. The nanogold modified electrode exhibited a higher peak current attributed to the increased surface area of the electrode when compared to the unmodified electrode. An increase in hysteresis was also observed. This diffusive limited behavior arose from analyte diffusion profiles at each band, in the IDE, overlapping resulting in the IDE behaving as a larger electrode. Figure 4 (a) and (b) shows typical CV from a modified and unmodified electrode undertaken at different scan rates. The near overlap of peak currents is indicative of semi-steady state behavior as occurs at low scan rates of these ultra-microelectrodes. The measure peak currents presented in Figure 4(b) following deposition of gold deposition show a significant increase when compared to the unmodified electrodes. This may be attributed to the increased surface area of the modified electrodes as agrees with previous report [51].

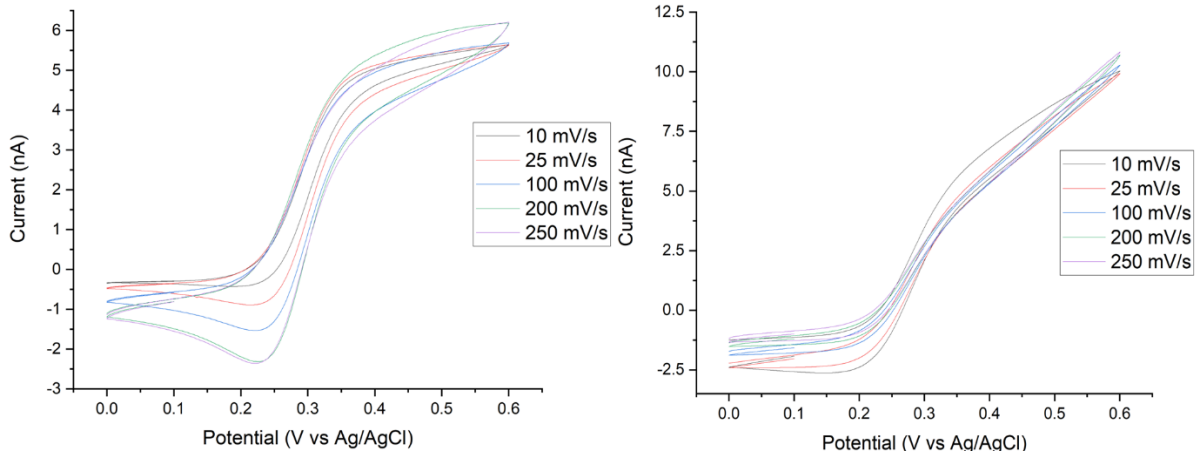

Fig.4 CV profiles of the WE using Ferrocine before (left) and after (right) the chropotentiometric deposition and the AuCl enriched WE after the detection of 256 nM of Ethidium Bromide.

We initially investigated the use CV as the electroanalytical method of choice for EtBr in the voltage range of -00.6 to 0.6 at 100 mV/s. However, no well defined peaks were observed. To this end, square wave voltammetry 22 mV/s and 10 mV amplitude was employed. The use of a platinum on-chip

reference electrode, over commercial Ag/AgCl reference electrodes, was preferred as it is solid-state and removed the need for any additional electrodes.[52]. Figure 5 (a) shows typical SWV obtained for different concentrations of EtBR. Well defined peaks, proportional to EtBr concentration, were observed at ~0.5v. Figure 5(a) shows a calibration curve plotted using the SWV peak currents presented in figure 5(b). Three different sensors were used for each concentration and, although tiny, the error bars are included in the data. Each data point represents the mean of three replicates and the error bars represent one standard deviation. The calibration curve resulted in a R^2 of 0.99 with a sensitivity (slope) of 1.5 pA/pM The theoretical LOD was calculated as 12 nM using the equation 3xSD/slope which is significantly lower than the reported literature [18].

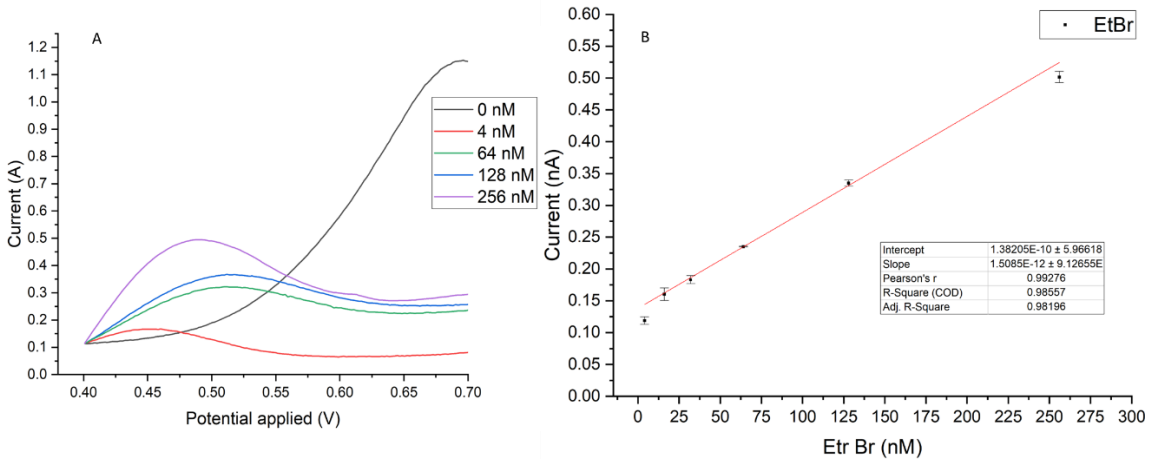

Fig.5 (a) Calibration curve for the different concentrations of EtBr (nM), with an LOD of 12 nM, (b) SWV profiles of the different concentration of [Ethidium bromide]

The SWV in figure 5 (a) exhibited a higher background current (possibly capacitive) after the EtBr oxidation event. This suggests that the redox process was influencing / modifying the electrode in some manner possibly by electrodepositing at an electrode surface. This is known to happen at commercial macroscale glassy carbon electrodes; that are typically polished between measurements to remove any bound material. To understand if this was the case with gold electrode, we undertook further AFM analysis.

Figure 6 shows AFM images of a portion of a gold electrode prior to (left), and, after (right) EtBr detection. As can be seen, there is no clear difference in the two profiles heights but there is other than a slight reduction in the root means square roughness of the electrode, suggesting that if a

passivation layer is present then it is extremely thin and that the as the heights didn't change the deposited gold did not delaminate from the electrode surface.

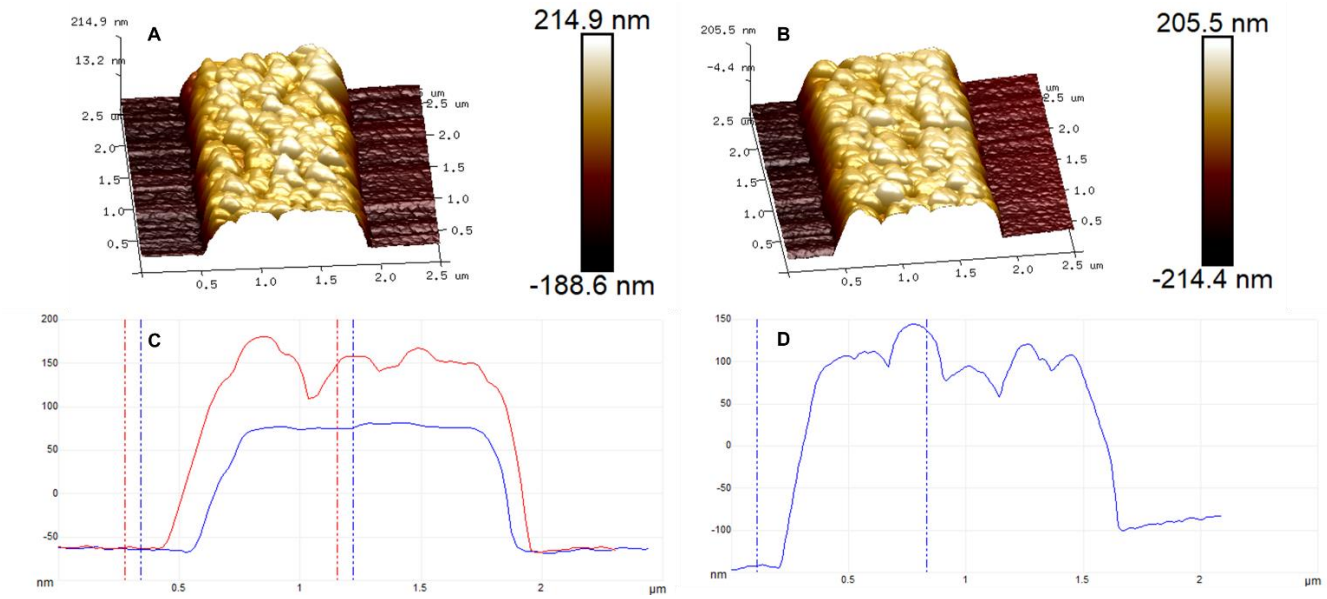

Fig.6 (A + C) AFM profile of a session of working electrode after the chronopotentiometric deposition, (B + D) profile comparison between undeposited (blue) and deposited working electrode's rode.

To confirm the presence of a passivation layer and elucidate changes in electrode behavior, CV and electrochemical impedance spectroscopy was undertaken at electrodes both pre and post EtBr detection in 5 mM FCA. The CV data presented in Figure 7(a) exhibited a significant decrease in current falling from ~12 nA to ~0.5nA following EtBr analysis. The observed hysteresis arises from capacitive charging of the electrode [44]. These results strongly suggest that a passivation layer is present. This is further supported by the EIS data presented in Figure 7(b) where the charge transfer resistance was observed to increase from ~100 kΩ for pre-ETtBR detection to 60 MΩ for post EtBr detection, which is clearly indicative of the presence of a passivation layer coating the electrode. It was observed that this passivation layer could not be removed by potentiodynamically cleaning approaches, indicating that the sensors are single use only.

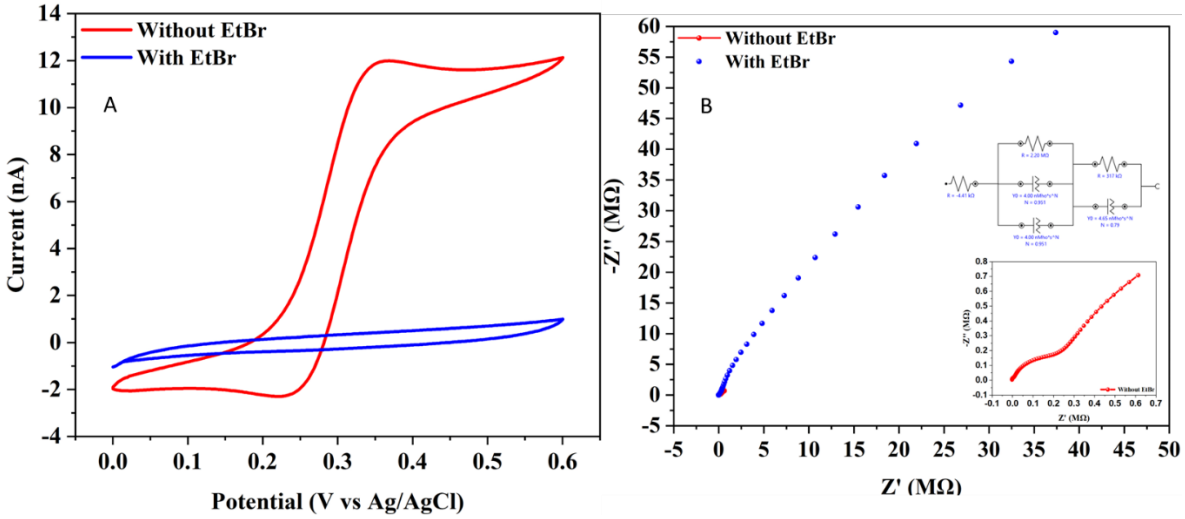

Fig. 7 Impedence profile of the sensor using Ferrocine 1 uM in PBS in different condition of deposition: after the Gold deposition using the previously described Chronopotentiometric protocol and after the detection of 256 nM of Ethidium Bromide; fig. A Use the CV using the previously protocol for Ferrocine deposition, fig. B is an impedence profile with the the circuit deduct using the potentiostat ANOVA software

To explore the applicability of the electrodes for EtBr detection, swabs were taken from different locations of a microbiology laboratory which regularly uses EtBr, a fluorescent label for nucleic acid detection. Three locations were selected where the potential for detecting EtBr was zero, low, and high, mainly: the post electrophoresis gel tray, the TAE (Tris-acetate-EDTA) buffer tray and the gel preparation fume hood and analyzed as described in the experimental section. Representative CVs with an image of the swabbed area are presented in Figure 8. As expected, zero or very low concentrations of EtBr were measured for the swabs taken from outside the fume hood. A significant concentration was measured for swabs taken inside the fume cupboard corresponding to ~250 nM of EtBr. This means that significant concentrations of EtBr remain on these surfaces despite UV and cleaning protocols. These results are important as they can inform the preparation of occupational risk assessments highlighting contaminated areas within a laboratory.

We field-tested the sensor on three different surfaces of a biotechnology lab with a long history of using EtBr for electrophoresis related activity. The first sample is the surface of the fume hood, used specifically to prepare agarose gels with EtBr, thus it has a high risk of contamination being an area of intense activity in which the solution is used in its stock concentration. The second sample is the basin of exhausted gel, a surface which presents a moderate risk of contamination due to the leaks from the melting gel but mitigated by the UV exposure applied to the gels themselves. The last reading is an electrophoretic gel basin before use and therefore well cleaned a couple of days before.

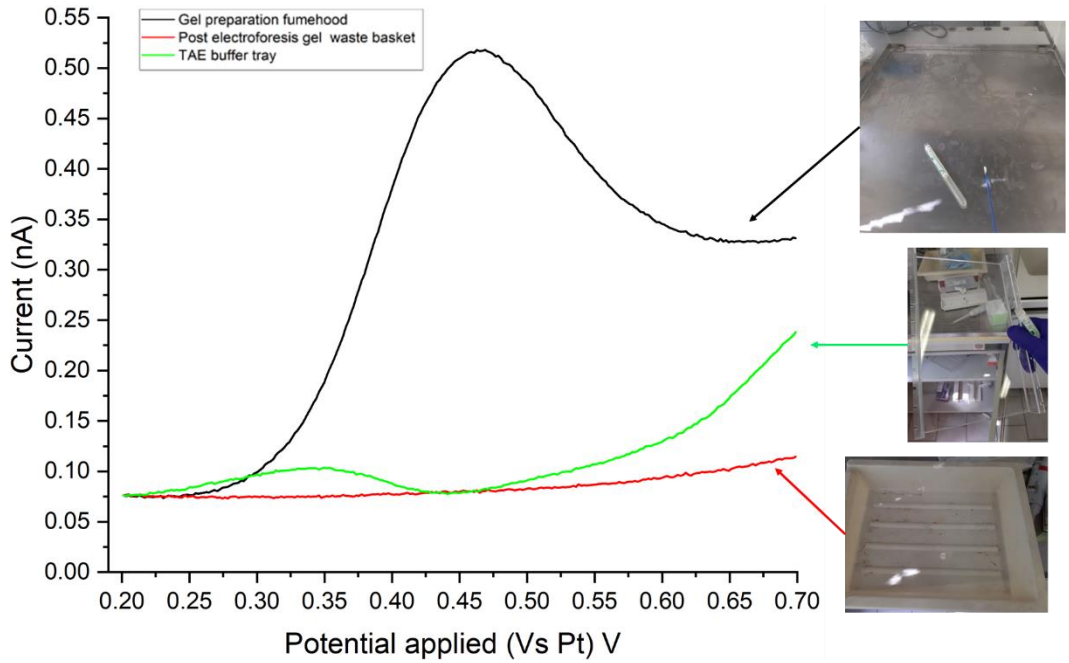

Fig. 8 Images from the surfaces of the laboratory, which samples has been took and their relative risk of contamination due to different level of exposition and cleaning frequency. In (d) the graph with the curve together

Due to the limit of the SEM we also check the structure changes in the working electrodes before and after the exposure to Ethidium bromide, the data collected suggested a slightly decrease in roughness and volume relatable to the electrical current activity rather than a corrosion operated by the Solution or due to a potential binding between the component of the Ethidium Bromide and the surface. (Fig.8)

Conclusion

EtBr is commonly used in molecular biology labs and poses a risk to healthy and safety due to its potential mutagenic properties. In this paper we explored the possibility to develop an electrochemical sensor tailored for the reality of busy molecular biology labs in which the risk of spills related to the EtBr can still be considered a threat.

Using IDF electrochemical technology it has been proved possible to detect EtBr from an microbiology lab surface with a sensibility lower than the strict 12 nM concentration as required by the European law[27], the LoD of 12 nM represent also at the moment an important milestone to the use of EtBr as electrochemical probe for PCR-free procedures that usually operate between 10^{-9} and 10^{-8} nM of nucleic acids.

Further development will also focus on the ability to reuse the working electrode and improve the sensibility of the chip.

ACKNOWLEDGMENTS

This publication has emanated from research supported by a research grant from Science Foundation Ireland under SFi SFI-17/CDA/4717 and from Science Foundation Ireland and the Department of Agriculture, Food and Marine on behalf of the Government of Irelandunder the Grant 16/RC/3835 (VistaMilk)

Bibliography

[1] L. M. Tumir, M. R. Stojković, and I. Piantanida, 'Come-back of phenanthridine and phenanthridinium derivatives in the 21st century', *Beilstein J. Org. Chem.*, vol. 10, pp. 2930–2954, Dec. 2014, doi: 10.3762/bjoc.10.312.

[2] J. Matić *et al.*, 'DNA/RNA recognition controlled by the glycine linker and the guanidine moiety of phenanthridine peptides', *Int. J. Biol. Macromol.*, vol. 134, pp. 422–434, Aug. 2019, doi: 10.1016/j.ijbiomac.2019.05.063.

[3] D. Saftić *et al.*, 'Impact of linker between triazolyluracil and phenanthridine on recognition of DNA and RNA. Recognition of uracil-containing RNA', *New J. Chem.*, vol. 41, no. 22, pp. 13240–13252, 2017, doi: 10.1039/c7nj02699d.

[4] M. J. Waring, 'Complex formation with DNA and inhibition of Escherichia coli RNA polymerase by ethidium bromide', *Biochim. Biophys. Acta BBA - Spec. Sect. Nucleic Acids Relat. Subj.*, 1964, doi: https://doi.org/10.1016/0926-6550(64)90238-5.

[5] J. Olmsted III and D. R. Kearns, 'ETHIDIUM FLUORESCENCE ENHANCEMENT MECHANISM Mechanism of Ethidium Bromide Fluorescence Enhancement on Binding to Nucleic Acids1"', Springer-Verlag, p 21. Umezawa, H, 1972. [Online]. Available: https://pubs.acs.org/sharingguidelines

[6] J. Olmsted and D. R. Kearns, 'Biomedicine 18, 459. Umezawa, H. (1979, in Antibiotics 111', Springer-Verlag, 1968.

[7] F. Diaz, M. Pilar Bayona-Bafaluy, M. Rana, M. Mora, H. Hao, and C. T. Moraes, 'Human mitochondrial DNA with large deletions repopulates organelles faster than full-length genomes under relaxed copy number control'.

[8] K. Lalchhandama, 'The making of modern biotechnology: how ethidium bromide made fame'. [Online]. Available: www.sciencevision.org

[9] E. Rampacci *et al.*, 'Ethidium bromide exposure unmasks an antibiotic efflux system in Rhodococcus equi', *J. Antimicrob. Chemother.*, vol. 76, no. 8, pp. 2040–2048, Aug. 2021, doi: 10.1093/jac/dkab121.

[10] B. B. A Newton, 'The Mode of Action of Phenanthridines: The Effect of Ethidiurn Bromide on Cell Division and Nucleic Acid Synthesis', 1957.

[11] M. M. K. Nasst, 'Abnormal DNA Patterns in Animal Mitochondria: Ethidium Bromide-Induced Breakdown of Closed Circular DNA and Conditions Leading to Oligomer Accumulation*', 1970. [Online]. Available: https://www.pnas.org

[12] P. Desjardins, E. Frost, and R. Morais1, 'Ethidium Bromide-Induced Loss of Mitochondrial DNA from Primary Chicken Embryo Fibroblasts', 1985. [Online]. Available: https://journals.asm.org/journal/mcb

[13] T. Nacarelli, A. Azar, and C. Sell, 'Inhibition of mTOR prevents ROS production initiated by ethidium bromide-induced mitochondrial DNA depletion', *Front. Endocrinol.*, vol. 5, no. JUL, 2014, doi: 10.3389/fendo.2014.00122.

[14] L. I. Hernandez, M. Zhong, S. H. Courtney, L. A. Marky, and N. R. Kallenbach, 'Equilibrium Analysis of Ethidium Binding to DNA Containing Base Mismatches and Branches', *Biochemistry*, vol. 33, no. 44, pp. 13140–13146, Nov. 1994, doi: 10.1021/bi00248a025.

[15] Y. Song *et al.*, 'A New Strategy to Reduce Toxicity of Ethidium Bromide by Alternating Anions: New Derivatives with Excellent Optical Performances, Convenient Synthesis, and Low Toxicity', *Small Methods*, vol. 4, no. 3, Mar. 2020, doi: 10.1002/smtd.201900779.

[16] R. Galindo-Murillo and T. E. Cheatham, 'Ethidium bromide interactions with DNA: An exploration of a classic DNA-ligand complex with unbiased molecular dynamics simulations', *Nucleic Acids Res.*, vol. 49, no. 7, pp. 3735–3747, Apr. 2021, doi: 10.1093/nar/gkab143.

[17] N. C. Garbett, N. B. Hammond, and D. E. Graves, 'Influence of the amino substituents in the interaction of ethidium bromide with DNA', *Biophys. J.*, vol. 87, no. 6, pp. 3974–3981, 2004, doi: 10.1529/biophysj.104.047415.

[18] S. C. B. Oliveira and V. B. Nascimento, 'Electrochemical oxidation mechanism of ethidium bromide at a glassy carbon electrode', *Electroanalysis*, vol. 25, no. 9, pp. 2117–2123, 2013, doi: 10.1002/elan.201300222.
[19] C. Zhang, L. Liu, J. Wang, F. Rong, and D. Fu, 'Electrochemical degradation of ethidium bromide using boron-doped diamond electrode', *Sep. Purif. Technol.*, vol. 107, pp. 91–101, 2013, doi: 10.1016/j.seppur.2013.01.033.
[20] I. C. Gherghi, S. T. Girousi, A. N. Voulgaropoulos, and R. Tzimou-Tsitouridou, 'Study of interactions between DNA-ethidium bromide (EB) and DNA-acridine orange (AO), in solution, using hanging mercury drop electrode (HMDE)', *Talanta*, vol. 61, no. 2, pp. 103–112, Oct. 2003, doi: 10.1016/S0039-9140(03)00238-8.
[21] X. Sun, P. He, S. Liu, J. Ye, and Y. Fang, 'Immobilization of single-stranded deoxyribonucleic acid on gold electrode with self-assembled aminoethanethiol monolayer for DNA electrochemical sensor applications', 1998.
[22] R. A. M. S. Corrêa, F. S. Da Cruz, C. C. Santos, T. C. Pimenta, D. L. Franco, and L. F. Ferreira, 'Optimization and application of electrochemical transducer for detection of specific oligonucleotide sequence for mycobacterium tuberculosis', *Biosensors*, vol. 8, no. 3, 2018, doi: 10.3390/bios8030084.
[23] A. E.-D. Salah El-Din, S. Abdullah, and A. E.-D. H. Sayed, 'Antioxidant capacity and DNA damage in Nile tilapia (Oreochromis niloticus) exposed to Ethidium bromide: A protective role for Spirulina Platensis', *Sci. Afr.*, vol. 13, p. e00961, Sep. 2021, doi: 10.1016/j.sciaf.2021.e00961.
[24] N. Von Wurmb-Schwark, L. Cavelier, and G. A. Cortopassi, 'A low dose of ethidium bromide leads to an increase of total mitochondrial DNA while higher concentrations induce the mtDNA 4997 deletion in a human neuronal cell line', *Mutat. Res. Mol. Mech. Mutagen.*, vol. 596, no. 1–2, pp. 57–63, Apr. 2006, doi: 10.1016/j.mrfmmm.2005.12.003.
[25] R. B. Uera, A. M. Paz-Alberto, and G. C. Sigua, 'Phytoremediation potentials of selected tropical plants for Ethidium bromide', *Environ. Sci. Pollut. Res. - Int.*, vol. 14, no. 7, pp. 505–509, Nov. 2007, doi: 10.1065/espr2007.02.391.
[26] M. Miko and B. Chance, 'Ethidium bromide as an uncoupler of oxidative phosphorylation', *FEBS Lett.*, vol. 54, no. 3, pp. 347–352, Jul. 1975, doi: 10.1016/0014-5793(75)80937-9.
[27] M. Lange and P. May, 'Effects of ethidium bromide on the production of ribosomal RNA in cultured mouse cells', *Nucleic Acids Res.*, vol. 6, no. 8, pp. 2863–2877, 1979, doi: 10.1093/nar/6.8.2863.
[28] F. M. Yakes and B. Van Houten, 'Mitochondrial DNA damage is more extensive and persists longer than nuclear DNA damage in human cells following oxidative stress', *Proc. Natl. Acad. Sci.*, vol. 94, no. 2, pp. 514–519, Jan. 1997, doi: 10.1073/pnas.94.2.514.
[29] A. S. Bess, T. L. Crocker, I. T. Ryde, and J. N. Meyer, 'Mitochondrial dynamics and autophagy aid in removal of persistent mitochondrial DNA damage in Caenorhabditis elegans', *Nucleic Acids Res.*, vol. 40, no. 16, pp. 7916–7931, Sep. 2012, doi: 10.1093/nar/gks532.
[30] Z. Rong *et al.*, 'The Mitochondrial Response to DNA Damage', *Front. Cell Dev. Biol.*, vol. 9, p. 669379, May 2021, doi: 10.3389/fcell.2021.669379.
[31] L. J. Niedernhofer, A. U. Gurkar, Y. Wang, J. Vijg, J. H. J. Hoeijmakers, and P. D. Robbins, 'Nuclear Genomic Instability and Aging', *Annu. Rev. Biochem.*, vol. 87, no. 1, pp. 295–322, Jun. 2018, doi: 10.1146/annurev-biochem-062917-012239.
[32] E. Seli, T. Wang, and T. L. Horvath, 'Mitochondrial unfolded protein response: a stress response with implications for fertility and reproductive aging', *Fertil. Steril.*, vol. 111, no. 2, pp. 197–204, Feb. 2019, doi: 10.1016/j.fertnstert.2018.11.048.
[33] G. N. Cecchino, E. Seli, E. L. Alves Da Motta, and J. A. García-Velasco, 'The role of mitochondrial activity in female fertility and assisted reproductive technologies: overview and current insights', *Reprod. Biomed. Online*, vol. 36, no. 6, pp. 686–697, Jun. 2018, doi: 10.1016/j.rbmo.2018.02.007.

[34] X.-L. Wang *et al.*, 'Mitophagy, a Form of Selective Autophagy, Plays an Essential Role in Mitochondrial Dynamics of Parkinson's Disease', *Cell. Mol. Neurobiol.*, vol. 42, no. 5, pp. 1321–1339, Jul. 2022, doi: 10.1007/s10571-021-01039-w.
[35] M. Boguenet, P.-E. Bouet, A. Spiers, P. Reynier, and P. May-Panloup, 'Mitochondria: their role in spermatozoa and in male infertility', *Hum. Reprod. Update*, vol. 27, no. 4, pp. 697–719, Jun. 2021, doi: 10.1093/humupd/dmab001.
[36] G. Lunn and E. B. Sansone, 'Ethidium Bromide: Destruction and Decontamination of Solutions1v2', 1987.
[37] S. Singh, N. Singh, and A. N. Singh, 'Ethidium bromide: Is a stain turning into a pollutant? A synthesis on its status, waste management, monitoring challenges and ecological risks to the environment', *Int. J. Res. Anal. Rev.*, vol. 5, 2018, [Online]. Available: https://www.researchgate.net/publication/341524958
[38] A. Debroy, M. Yadav, R. Dhawan, S. Dey, and N. George, 'DNA dyes: toxicity, remediation strategies and alternatives', *Folia Microbiol. (Praha)*, vol. 67, no. 4, pp. 555–571, Aug. 2022, doi: 10.1007/s12223-022-00963-8.
[39] R. Sulthana, S. N. Taqui, F. Zameer, U. T. Syed, and A. A. Syed, 'Adsorption of ethidium bromide from aqueous solution onto nutraceutical industrial fennel seed spent: Kinetics and thermodynamics modeling studies', *Int. J. Phytoremediation*, vol. 20, no. 11, pp. 1075–1086, Sep. 2018, doi: 10.1080/15226514.2017.1365331.
[40] Saruchi, R. Verma, V. Kumar, and A. A. ALOthman, 'Comparison between removal of Ethidium bromide and eosin by synthesized manganese (II) doped zinc (II) sulphide nanoparticles: kinetic, isotherms and thermodynamic studies', *J. Environ. Health Sci. Eng.*, vol. 18, no. 2, pp. 1175–1187, 2020, doi: 10.1007/s40201-020-00536-2.
[41] C. Weeraphan *et al.*, 'Application of the Magnetic Fraction of Fly Ash as a Low-Cost Heterogeneous Fenton Catalyst for Degrading Ethidium Bromide', *Anal. Lett.*, vol. 55, no. 6, pp. 965–979, Apr. 2022, doi: 10.1080/00032719.2021.1977313.
[42] D. Lowe, 'The Myth of Ethidium Bromide', 2016. [Online]. Available: http://blogs.sciencemag.org/pipeline/archives/2016/04/18/the-myth-of-ethidium-bromide
[43] B. O'Sullivan *et al.*, 'A simulation and experimental study of electrochemical pH control at gold interdigitated electrode arrays', *Electrochimica Acta*, vol. 395, Nov. 2021, doi: 10.1016/j.electacta.2021.139113.
[44] I. Seymour, B. O'Sullivan, P. Lovera, J. F. Rohan, and A. O'Riordan, 'Electrochemical detection of free-chlorine in Water samples facilitated by in-situ pH control using interdigitated microelectrodes', *Sens. Actuators B Chem.*, vol. 325, Dec. 2020, doi: 10.1016/j.snb.2020.128774.
[45] N. Moukri, B. Patella, C. Cipollina, E. Pace, A. O'Riordan, and R. Inguanta, 'Electrochemical detection of human Immunoglobulin-G using Gold Nanowires Immunosensor', in *2023 IEEE BioSensors Conference, BioSensors 2023 - Proceedings*, Institute of Electrical and Electronics Engineers Inc., 2023. doi: 10.1109/BioSensors58001.2023.10281025.
[46] I. Seymour, B. O'Sullivan, P. Lovera, J. F. Rohan, and A. O'Riordan, 'Elimination of Oxygen Interference in the Electrochemical Detection of Monochloramine, Using *In Situ* pH Control at Interdigitated Electrodes', *ACS Sens.*, vol. 6, no. 3, pp. 1030–1038, Mar. 2021, doi: 10.1021/acssensors.0c02264.
[47] I. Seymour, B. O'Sullivan, P. Lovera, J. F. Rohan, and A. O'Riordan, 'Removal of Dissolved Oxygen Interference in the Amperometric Detection of Monochloramine Using a pH Control Method', in *2019 IEEE SENSORS*, Montreal, QC, Canada: IEEE, Oct. 2019, pp. 1–4. doi: 10.1109/SENSORS43011.2019.8956674.
[48] A. Murphy, I. Seymour, J. Rohan, A. OrRiordan, and I. OrConnell, 'Portable Data Acquisition System for Nano and Ultra-Micro Scale Electrochemical Sensors', *IEEE Sens. J.*, pp. 1–1, 2020, doi: 10.1109/JSEN.2020.3021941.

[49] R. Daly, T. Narayan, H. Shao, A. O'Riordan, and P. Lovera, 'Platinum-Based Interdigitated Micro-Electrode Arrays for Reagent-Free Detection of Copper', *Sensors*, vol. 21, no. 10, p. 3544, May 2021, doi: 10.3390/s21103544.
[50] G. Wang, J. Zhang, and R. W. Murray, 'DNA binding of an ethidium intercalator attached to a monolayer-protected gold cluster', *Anal. Chem.*, vol. 74, no. 17, pp. 4320–4327, 2002.
[51] L. A. Wasiewska *et al.*, 'Reagent free electrochemical-based detection of silver ions at interdigitated microelectrodes using in-situ pH control', *Sens. Actuators B Chem.*, vol. 333, p. 129531, Apr. 2021, doi: 10.1016/j.snb.2021.129531.
[52] Y. Seguí Femenias, U. Angst, F. Caruso, and B. Elsener, 'Ag/AgCl ion-selective electrodes in neutral and alkaline environments containing interfering ions', *Mater. Struct. Constr.*, vol. 49, no. 7, pp. 2637–2651, Jul. 2016, doi: 10.1617/s11527-015-0673-8.